RESEARCH ARTICLE | SEPTEMBER 03 2024

In-operando microwave scattering-parameter calibrated measurement of a Josephson traveling wave parametric amplifier ©

Special Collection: Advances in Quantum Metrology

S.-H. Shin ⁽¹⁾; M. Stanley ⁽²⁾; W. N. Wong ⁽³⁾; T. Sweetnam ⁽³⁾; A. Elarabi ⁽³⁾; T. Lindström ⁽³⁾; N. M. Ridler ⁽³⁾; S. E. de Graaf ⁽³⁾



Appl. Phys. Lett. 125, 104001 (2024) https://doi.org/10.1063/5.0220776





Articles You May Be Interested In

Traveling wave parametric amplifier with Josephson junctions using minimal resonator phase matching Appl. Phys. Lett. (June 2015)

A 4–8 GHz kinetic inductance traveling-wave parametric amplifier using four-wave mixing with near quantum-limited noise performance

Numerical analysis of a three-wave-mixing Josephson traveling-wave parametric amplifier with engineered dispersion loadings

J. Appl. Phys. (October 2022)

Challenge us.

What are your needs for periodic signal detection?



Find out more





Cite as: Appl. Phys. Lett. **125**, 104001 (2024); doi: 10.1063/5.0220776 Submitted: 28 May 2024 · Accepted: 20 August 2024 · Published Online: 3 September 2024







S.-H. Shin,^{1,2} (D) M. Stanley,¹ (D) W. N. Wong,¹ (D) T. Sweetnam,¹ (D) A. Elarabi,¹ (D) T. Lindström,¹ (D) N. M. Ridler,¹ (D) and S. E. de Graaf^{1,a)} (D)

AFFILIATIONS

¹National Physical Laboratory, Teddington TW11 OLW, United Kingdom

Note: This paper is part of the APL Special Collection on Advances in Quantum Metrology.

a) Author to whom correspondence should be addressed: sdg@npl.co.uk

ABSTRACT

Superconducting traveling wave parametric amplifiers (TWPAs) are broadband near-quantum limited microwave amplifiers commonly used for qubit readout and a wide range of other applications in quantum technologies. The performance of these amplifiers depends on achieving impedance matching to minimize reflected signals. Here, we apply a microwave calibration technique to extract the S-parameters of a Josephson junction based TWPA in-operando. This enables reflections occurring at the TWPA and its extended network of components to be quantified, and we find that the in-operation performance can be well described by the off-state measured S-parameters.

© 2024 Author(s). All article content, except where otherwise noted, is licensed under a Creative Commons Attribution-NonCommercial 4.0 International (CC BY-NC) license (https://creativecommons.org/licenses/by-nc/4.0/). https://doi.org/10.1063/5.0220776

Quantum limited parametric amplifiers are becoming essential components in measurement chains for solid-state quantum devices and quantum computers. Recent years have seen tremendous advances in parametric amplifier technology, ^{1–3} with a wide range of amplifier implementations ^{4–8} and numerous commercial alternatives emerging. Of particular interest is broadband traveling-wave parametric amplifiers (TWPAs) as they offer great flexibility when operating at typical frequencies for quantum circuits, while still providing a sufficient amount of gain and SNR improvement for many applications.

Due to their operation principles utilizing propagating microwaves, TWPAs are very sensitive to their environment and the auxiliary components used in the setup. In particular, accurate impedance matching is crucial to avoid spurious reflected signals being amplified, resulting in gain ripples and reduced overall gain for the signal of interest. To this end, a refined knowledge of the detailed microwave performance (S-parameters) under different operating conditions will enable further improvements in amplifier performance. Previous amplifier developments critically focused on SNR improvement and noise performance, commonly utilizing the Y-factor or other noise figure methods. The amplifier developments are typically based on short-open-load-through (SOLT) or thru-reflect-line

(TRL) calibration schemes. For millikelvin (mK) measurements, SOLT has a critical disadvantage: it requires pre-defined calibration standards at the operating temperature. This is often unfeasible at mK temperatures due to performance changes in the standards at these temperatures. In contrast, TRL standards do not need to be predefined. This makes TRL an attractive calibration scheme for mK temperatures, since it is generally unaffected by associated changes in the standards.

Here, we demonstrate how to evaluate the two-port scattering parameters (S-parameters) of a commercial Josephson junction-based TWPA (JTWPA, Silent-Waves Argo¹⁶) during operation at mK temperatures using a low RF power TRL calibration technique compatible with quantum circuit operation.^{17–20} We also independently carry out a calibrated measurement of the auxiliary circuitry required to operate the JTWPA. In this way, we obtain accurate S-parameter measurements for all the relevant driving conditions of the JTWPA. Our measurements can help inform improved impedance engineering as well as a detailed understanding of the impact from fabrication-induced parameter spread^{21,22} and external factors hampering TWPA performance.¹⁰

Non-idealities in the measurement setup caused by imperfect connectors and cabling will introduce errors in S-parameter

²Sejong University, Seoul 05006, Republic of Korea

measurements of the device under test (DUT). To measure the actual S-parameters at mK temperatures, a calibration scheme that shifts the reference planes to the input and output ports of the device is required, de-embedding the components between a room-temperature vector network analyzer (VNA) and the device at mK temperatures.

Our two-port S-parameter calibration setup has been specifically developed to characterize quantum circuits, which operate at very low power levels, ¹⁷ (<-100 dBm) and is shown in Fig. 1, together with the

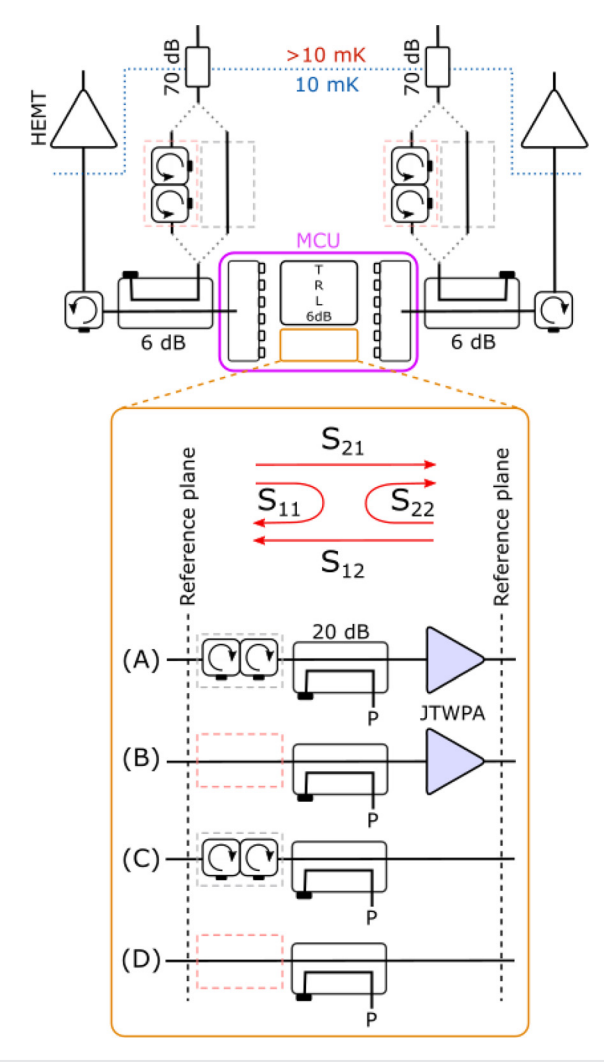


FIG. 1. Schematic of the mK S-parameter calibration setup and the DUT networks measured. The calibration reference planes are moved to the ports of the six-way cryogenic switches. Three ports are occupied by the TRL standards, at another port, we mount a well-characterized 6 dB cryogenic attenuator for additional validation of the calibration, and on the two remaining switch ports, we carried out measurements of the JTWPA, and it is auxiliary network as in configurations (A) and (C) and (B) and (D), in two separate cooldowns, respectively. Dashed boxes indicate that isolators are either part of the DUTs or mounted outside the switch reference planes. Two configurations are used in two separate cooldowns, either with double junction isolators within the reference planes, and thru lines at the input ports (grey dashed boxes), or the opposite with isolators moved to the input ports (red dashed boxes).

four device configurations measured (A–D). The cold microwave calibration unit (MCU) consists of two 6-way cryogenic RF switches that are used to select between the TRL calibration standards or the DUTs, and they define the location of the calibrated reference planes. We have previously characterized the uncertainty introduced by these switches to be <0.1 dB in transmission at mK. 23 The setup utilizes two heavily attenuated (50 dB) input lines and two output lines equipped with wideband (0.3–14 GHz) high electron mobility transistor (HEMT) amplifiers mounted on the 4 K stage of the cryostat. A two-stage room temperature amplification chain further brings the signals to an acceptable level for VNA receiver measurements.

The thru standard is a zero-length insertable through connection of the nominally identical coaxial cables between switches and standards/DUT. The reflect standards are commercial (Maury Microwave 8046F6) 3.5 mm coaxial connectorized male and female offset short standards. The reference impedance of the calibration is the characteristic impedance of the line standard, which has been measured to be very close to $50\,\Omega$ (49.94 \pm 0.03 Ω in the frequency range 2–8 GHz) and is temperature invariant from 25 mK to 296 K. 24 We have previously characterized the error budget of our setup, $^{23-25}$ finding a reflection coefficient uncertainty of about 0.04 in linear units (corresponding to an uncertainty of approximately 0.3 dB at a S-parameter magnitude of 0 dB, and an uncertainty of approximately 3 dB at a S-parameter magnitude of $-20\,\mathrm{dB}$).

All four uncalibrated S-parameters are obtained by measuring the respective RF input and output coaxial lines, which connect the MCU to a 4-port VNA (PNA-X N5247B). The JTWPA pump line (indicated "P" in Fig. 1) is configured with $6/10/10/6/10\,\mathrm{dB}$ attenuation at $50\,\mathrm{K}/4\,\mathrm{K}/800\,\mathrm{mK}/100\,\mathrm{mK}/10\,\mathrm{mK}$ stages of the fridge, respectively. For all the lines, we also use $0.25-10\,\mathrm{GHz}$ bandpass filters (not drawn) at the $10\,\mathrm{mK}$ stage. All measurements were carried out at the base temperature of $10\,\mathrm{mK}$.

Impedance matching and suppression of reflections are essential for good amplifier performance, and it is common practice to place isolators both before and after the TWPA. In the former case, it also protects a qubit sample from backaction due to pump leakage, and in the latter case, it reduces thermal photons leaking from the HEMT stage reaching the TWPA or quantum circuit. In all cases, we use a single junction isolator (4-8 GHz) on the output lines on the common port of the RF switches. On the input side of the JTWPA, we use a double junction isolator (4-8 GHz) as indicated in Fig. 1. In cases A and C, the isolator is placed just in front of the pump coupler, and the common input lines lack an isolator (red dashed boxes). In cases B and D, the same isolator is instead moved from within the reference planes to the input lines (red dashed boxes). In the latter case, the JTWPA input port thus sees both the single junction and double junction isolator (via the 6 dB coupler), with the 6-way switch being the main source of potential reflections. These two configurations were measured in two consecutive cooldowns. In all cases, the cables used in-between the components were ensured to be of the same length and type. In this work, we perform all the cold stage measurements in the frequency range of 4-8 GHz, limited by the bandwidth of the cryogenic isolators used. One complication for S-parameter measurements in this architecture is that if the isolators are placed inside the calibration reference planes, only limited information about the JTWPA can be obtained. On the other hand, if placed further from the JTWPA, there is a chance of introducing additional reflections that can be amplified

as a result of the almost unitary reverse transmission of the JTWPA. Therefore, an understanding of reflections occurring in the wider network of components is also crucial.

To extract the actual S-parameters of the DUT at mK temperatures, we solve the 8-term error model²⁶ applied to the uncalibrated S-parameters measured with the VNA. This model accounts for systematic errors, such as directivity, source match, and reflection tracking, which are generated due to reflections in the measurement setup. To validate the calibration process,²⁷ we also used the aforementioned cryogenic 6 dB attenuator as DUT in each cooldown. For all the measurements (unless otherwise mentioned), we use a low input power (-30 dBm on the VNA, <-110 dBm incident on the JTWPA) to ensure we are operating well below JTWPA gain compression.

In Fig. 2, we show the measured S-parameters of all four configurations shown in the schematic of Fig. 1. We clearly see that the insertion and return losses due to the directional coupler (4–12 GHz QMC-CRYOCOUPLER-20, used to inject the pump tone) and the cables connecting it to the JTWPA are small (<1 dB and \lesssim –20 dB, respectively; configuration D), and so we can neglect these components without affecting the conclusions of the JTWPA measurement.

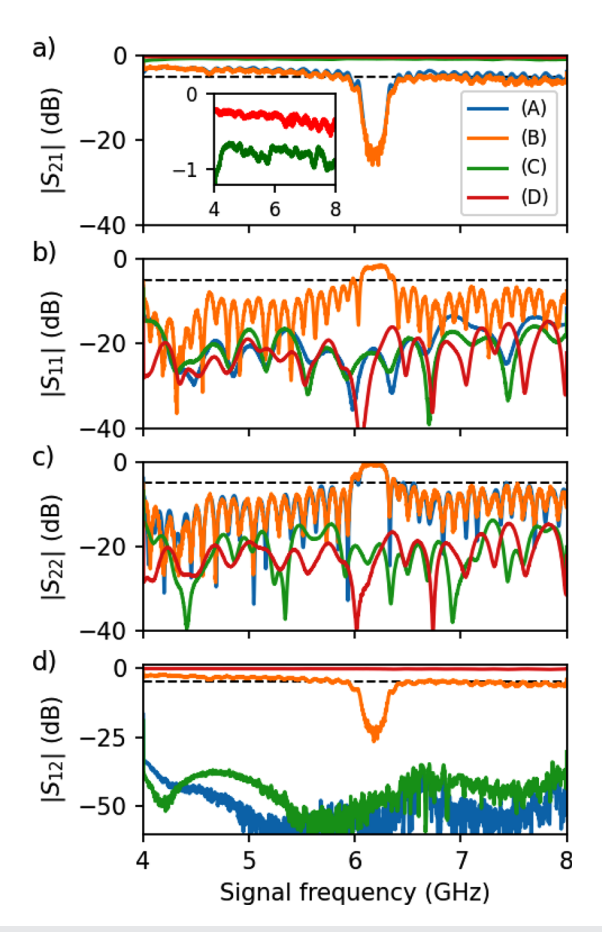


FIG. 2. S-parameters for configurations (A), (B), (C), and (D) obtained at 10 mK and typical DUT input signal levels of ≈ -110 dBm. The inset in (a) shows a close-up of the measured S_{21} response of the coupler and cables, and isolator, configurations (D) and (C), respectively. In all cases, the JTWPA pump tone is off. The horizontal dashed lines shows -5 dB as a reference.

Furthermore, we clearly suppress S_{11} [Fig. 2(b)] and reverse transmission [Fig. 2(d)] by inclusion of the isolator before the coupler [configuration (A) and (C)]. Thus, we can conclude that when we measure configuration (B), the response accurately represents the JTWPA performance alone.

When the pump tone is off, we measure an insertion loss of the JTWPA varying from 3 to 6 dB across the 4–8 GHz frequency range [Fig. 2(a)]. The reflection measured at the two ports [S_{11} , Fig. 2(b), and S_{22} , Fig. 2(c)] remains near or below -10 dB, indicating a device closely matched to 50 Ω .

Next, we turn on the JTWPA pump tone. In Fig. 3(a), we show an example of the measured S_{21} magnitude with the pump signal on and pump off. In what follows, we define this ratio between the pump on and pump off as $|S_{21}^{\rm on}|/|S_{21}^{\rm off}|$. This quantity should be compared to the actual ("useful") gain of the JTWPA relative to the case of no

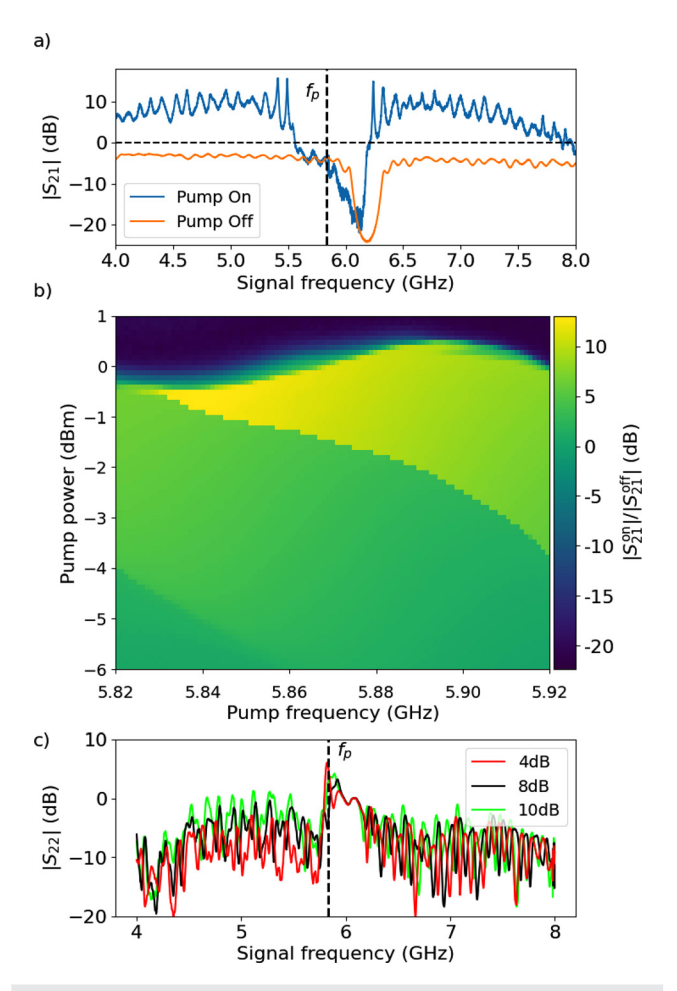


FIG. 3. In-operation performance. (a) Example S_{21} magnitude with the pump on and off (vertical dashed line at $f_{p}=5.8659\,\mathrm{GHz}$). Horizontal dashed line shows 0 dB as a reference. (b) Average pump on/off ratio $|S_{21}^{\mathrm{off}}|/|S_{21}^{\mathrm{off}}|$ as a function of pump power and frequency. (c) Typical examples of S_{22} at selected average $|S_{21}^{\mathrm{on}}|/|S_{21}^{\mathrm{off}}|$ ratios of 4 dB (taken at $P_{p}=-4.3\,\mathrm{dB},\,f_{p}=5.835\,\mathrm{GHz}$), 8 dB ($-1.5\,\mathrm{dB},\,5.02\,\mathrm{GHz}$), and 10 dB ($-1.5\,\mathrm{dB},\,5.875\,\mathrm{GHz}$). A moving average is used to better illustrate the overall trend of increasing S_{22} magnitude with increasing gain.

JTWPA at all, i.e., within our calibrated setup referenced to 0 dB. In Fig. 3(b), we show the $|S_{21}^{on}|/|S_{21}^{off}|$ ratio as a function of the pump frequency and power. The gain is averaged across all signal frequencies in the range of 4-8 GHz, excluding the stop band (5.5-6.5 GHz). In Fig. 3(c), we show selected S_{22} traces for different average $|S_{21}^{\text{on}}|/|S_{21}^{\text{off}}|$ ratios as a function of signal frequency, showing a clear overall increase in S_{22} with increasing gain. To quantify this in more detail, we show in Fig. 4(b) the change in the similarly averaged scattering parameters as a function of $|S_{21}^{\text{on}}|/|S_{21}^{\text{off}}|$. We see a significant increase in S_{11} and S_{22} , suggesting increased reflection from the device. This naively suggests that the impedance of the JTWPA transmission line changes with gain, however, as we will see this is a result of the initial impedance mismatch of the circuit, and the amplification of reflected signals. In the extreme cases, this gain results in reflected S-parameters exceeding 0 dB [Fig. 3(b)]. The impedance of the JTWPA itself is expected to change only by a very small amount under these pump conditions. 10

A simple model [sketched in Fig. 4(a)] can be used to investigate the behavior of S_{11} and S_{22} with increasing gain: similarly to the Fabry–Pérot cavity model described in Ref. 16, the system can be considered as two input/output ports with linear reflection coefficients r_1 and r_2 and transmissions t_1 and t_2 , with $[t_i^2 + r_i^2 = 1]_{i=1,2}$ in the lossless case. An incoming signal arrives at port 1 with a proportion r_1 being reflected back to the source and t_1 entering the amplifier. From here, the signal is amplified by the gain coefficient $g = \sqrt{G}$, with G the measured power gain, before being partially transmitted out of the amplifier through port 2, and partially reflected to stay within the

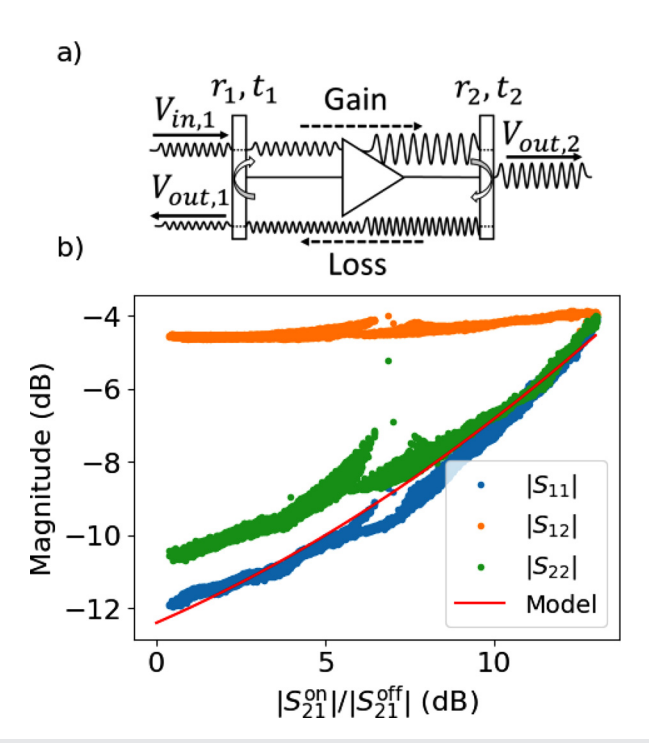


FIG. 4. S-parameters in the presence of gain. (a) Sketch of the setup used to model the role of reflected signals on the measured S-parameters of the JTWPA, see text for details. (b) Average S-parameter magnitude as a function of pump on/off ratio $|S_{21}^{\rm on}|/|S_{21}^{\rm off}|$. The solid line indicates the expected trend assuming the measured average S-parameters of the JTWPA pump off state and the model in (a).

amplifier. The signal continues to reflect back and forth within the amplifier, with a proportion transmitted at each port each time, while also being amplified between ports 1 and 2. The resulting ratio of the amplitudes of the output and input signal voltages from the arising geometric series can be expressed as

$$\frac{V_{out}}{V_{in}} = r_1 + \frac{t_1^2 g r_2}{1 - g r_2 r_1},\tag{1}$$

with the corresponding model for a signal arriving at port 2 obtained by swapping the subscripts. This model was used to calculate the average reflection coefficients from the pump-off S_{11} and S_{22} data in Fig. 2, assuming return loss of 3.5 dB as seen in the S_{21} data, producing values of $r_1 = r_2 \approx 0.14$. These reflection coefficients are used in Eq. (1) to calculate the expected change in S_{11} and S_{22} with increasing $|S_{21}^{\rm on}|/|S_{21}^{\rm off}|$ ratio, which is plotted in Fig. 4(b) and shows agreement within the measurement error.

This model is not able to distinguish reflections occurring directly at the JTWPA ports (internal) from reflections occurring further from the amplifier (external) or even outside the reference planes for calibration. We can conclude that external reflections do not play a major role since inclusion of the isolator within the reference planes (case A) has no significant effect on the change in S_{22} vs gain (S_{11} becomes inaccessible). Furthermore, case D shows that the coupler and cables used within the reference planes are well matched (Fig. 1). Hence, we conclude that the response in Fig. 4 must be dominated by internal reflections at the JTWPA ports.

Knowing the reflection coefficient allows, together with knowledge of the pump power, to estimate the amount of isolation required to reduce the reflected pump tone reaching the sample in front of the TWPA to the desired level.

All previous data were taken with a very low input signal power to the DUT (≈ -110 dBm) to ensure measurements were performed without saturating the JTWPA. As the last step, we characterize the response of the JTWPA as we increase the input signal power and start to observe gain compression. The magnitude of the S-parameters for a number of different signal powers is shown in Fig. 5, taken at a point near maximum gain ($|S_{21}^{\rm on}|/|S_{21}^{\rm off}| \sim 11$ dB; $f_p = 5.8659$ GHz, $P_p = -0.7$ dBm). These measurements confirm that previous measurements were done with a sufficiently low signal power to avoid any effects due to saturation. As the overall gain is suppressed by the signal power, we observe a non-trivial dependence of the reflection at the two ports [Fig. 5(d)], uncorrelated with the gain suppression [Fig. 5(c)]. Furthermore, S_{12} also drops sharply when the gain is significantly suppressed. Together, this indicates that the signal saturation results in changes to the devices intrinsic dissipation.

Measurements of S-parameters of a TWPA presents a challenge due to its non-linear and near-reciprocal response. Ideal operation seeks to minimize reflections utilizing isolators close to each port of the TWPA; however, inclusion of isolators obscures the TWPA response in calibrated measurements. Future calibrations methods would benefit from more advanced techniques such as also measuring the absolute power incident on the two ports, ²⁸ intermodulation distortion, ²⁹ or X-parameters and large-signal analysis, ³⁰ and will help inform more advanced TWPA engineering incorporating, e.g., reverse isolation. ^{31,32}

In summary, we have performed *in situ*, in-operando microwave S-parameter measurements of a JTWPA and its auxiliary network of components in a calibrated setup. We reveal how the S-parameters of

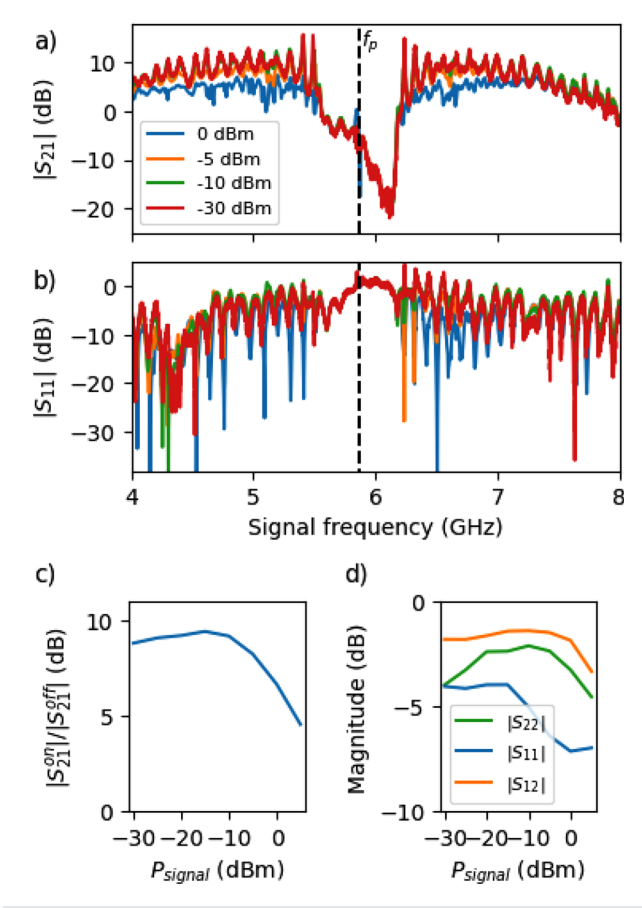


FIG. 5. Performance near gain compression. (a) S_{21} and (b) S_{11} magnitude vs signal frequency as a function of signal power (referenced to VNA output) taken with the pump tuned close to maximum gain (vertical dashed line at $f_p=5.8659\,\mathrm{GHz}$, $P_p=-0.7\,\mathrm{dBm}$). (c) The average $|S_{21}^\mathrm{con}|/|S_{21}^\mathrm{con}|$ ratio in the band 4.0–5.5 and 6.5–8.0 GHz as a function of signal power (referenced to the generator output level). (d) Average change in S-parameters as a function of signal power evaluated in the same frequency band.

the JTWPA depend on the strength of the pump and signal power, allowing us to understand how reflections influence the JTWPA performance and show how the JTWPA off-state S-parameters can accurately describe the on-state behavior. Our method allows to develop detailed models of the device physics based on the observed device characteristics and fine-tune parametric amplifier design to improve performance.

We acknowledge fruitful discussions with Luca Planat and Silent Waves. We acknowledge the support from the UK Department for Science, Innovation and Technology through the UK National Quantum Technologies Programme (NQTP). We also acknowledge support from the Engineering and Physical Sciences Research Council (EPSRC) (Grant No. EP/W027526/1).

AUTHOR DECLARATIONS Conflict of Interest

The authors have no conflicts to disclose.

Author Contributions

S.-H. Shin: Data curation (lead); Formal analysis (equal); Investigation (supporting); Methodology (supporting); Software (lead); Writing review & editing (supporting). M. Stanley: Data curation (supporting); Formal analysis (supporting); Investigation (equal); Methodology (equal); Resources (lead); Software (supporting); Supervision (supporting); Validation (lead); Writing - original draft (supporting); Writing - review & editing (supporting). W. N. Wong: Formal analysis (equal); Software (supporting); Writing - original draft (supporting); Writing review & editing (supporting). T. Sweetnam: Formal analysis (equal); Validation (supporting); Visualization (supporting); Writing – original draft (supporting); Writing - review & editing (supporting). A. Elarabi: Formal analysis (supporting); Investigation (supporting); Supervision (supporting); Writing - review & editing (supporting). T. Lindström: Conceptualization (supporting); Supervision (supporting); Validation (supporting); Writing – review & editing (supporting). N. M. Ridler: Conceptualization (supporting); Formal analysis (supporting); Investigation (supporting); Methodology (equal); Supervision (supporting); Validation (equal); Writing - review & editing (supporting). S. E. de Graaf: Conceptualization (lead); Formal analysis (supporting); Investigation (equal); Methodology (equal); Resources (supporting); Supervision (lead); Validation (supporting); Writing original draft (equal); Writing - review & editing (lead).

DATA AVAILABILITY

The data that support the findings of this study are openly available in Zenodo at https://doi.org/10.5281/zenodo.13268665, Ref. 33.

REFERENCES

¹C. Macklin, K. O'Brien, D. Hover, M. E. Schwartz, V. Bolkhovsky, X. Zhang, W. D. Oliver, and I. Siddiqi, Science **350**, 307 (2015).

²M. Esposito, A. Ranadive, L. Planat, and N. Roch, Appl. Phys. Lett. 119, 120501 (2021).

³M. Malnou and J. Aumentado, IEEE Trans. Microwave Theory Tech. **72**, 2158 (2024).

⁴B. H. Eom, P. K. Day, H. G. Leduc, and J. Zmuidzinas, Nat. Phys. **8**, 623–627

⁵A. A. Adamyan, S. E. de Graaf, S. E. Kubatkin, and A. V. Danilov, J. Appl. Phys. 119, 083901 (2016).

⁶D. Phan, P. Falthansl-Scheinecker, U. Mishra, W. Strickland, D. Langone, J. Shabani, and A. Higginbotham, Phys. Rev. Appl. **19**, 064032 (2023).

⁷F. Faramarzi, R. Stephenson, S. Sypkens, B. H. Eom, H. LeDuc, and P. Day, APL Quantum 1, 036107 (2024).

⁸J. Y. Qiu, A. Grimsmo, K. Peng, B. Kannan, B. Lienhard, Y. Sung, P. Krantz, V. Bolkhovsky, G. Calusine, D. Kim, A. Melville, B. M. Niedzielski, J. Yoder, M. E. Schwartz, T. P. Orlando, I. Siddiqi, S. Gustavsson, K. P. O'Brien, and W. D. Oliver, Nat. Phys. 19, 706–713 (2023).

⁹S. Kern, P. Neilinger, E. Il'ichev, A. Sultanov, M. Schmelz, S. Linzen, J. Kunert, G. Oelsner, R. Stolz, A. Danilov, S. Mahashabde, A. Jayaraman, V. Antonov, S. Kubatkin, and M. Grajcar, Phys. Rev. B 107, 174520 (2023)

¹⁰H. Renberg Nilsson, D. Shiri, R. Rehammar, A. Fadavi Roudsari, and P. Delsing, Phys. Rev. Appl. 21, 064062 (2024).

¹¹S. Simbierowicz, V. Vesterinen, J. Milem, A. Lintunen, M. Oksanen, L. Roschier, L. Grönberg, J. Hassel, D. Gunnarsson, and R. E. Lake, Rev. Sci. Instrum. 92, 034708 (2021).

¹²M. Malnou, T. F. Q. Larson, J. D. Teufel, F. Lecocq, and J. Aumentado, Rev. Sci. Instrum. 95, 034703 (2024).

¹³ A. Ranadive, M. Esposito, L. Planat, E. Bonet, C. Naud, O. Buisson, W. Guichard, and N. Roch, Nat. Commun. 13, 1737 (2022).

- ¹⁴M. R. Perelshtein, K. V. Petrovnin, V. Vesterinen, S. Hamedani Raja, I. Lilja, M. Will, A. Savin, S. Simbierowicz, R. N. Jabdaraghi, J. S. Lehtinen, L. Grönberg, J. Hassel, M. P. Prunnila, J. Govenius, G. S. Paraoanu, and P. J. Hakonen, Phys. Rev. Appl. 18, 024063 (2022).
- ¹⁵S. Simbierowicz, V. Y. Monarkha, S. Singh, N. Messaoudi, P. Krantz, and R. E. Lake, Appl. Phys. Lett. **120**, 054004 (2022).
- ¹⁶L. Planat, A. Ranadive, R. Dassonneville, J. Puertas Martínez, S. Léger, C. Naud, O. Buisson, W. Hasch-Guichard, D. M. Basko, and N. Roch, Phys. Rev. X 10, 021021 (2020).
- ¹⁷M. Stanley, S. E. de Graaf, T. Hönigl-Decrinis, T. Lindström, and N. M. Ridler, IEEE Access 10, 43376 (2022).
- ¹⁸M. Stanley, R. Parker-Jervis, S. de Graaf, T. Lindström, J. E. Cunningham, and N. M. Ridler, Electron. Lett. 58, 614 (2022).
- ¹⁹L. Ranzani, L. Spietz, Z. Popovic, and J. Aumentado, Rev. Sci. Instrum. 84, 034704 (2013).
- 20 L. Ranzani, S. Kotler, A. J. Sirois, M. P. DeFeo, M. Castellanos-Beltran, K. Cicak, L. R. Vale, and J. Aumentado, Phys. Rev. Appl. 8, 054035 (2017).
- ²¹C. Kissling, V. Gaydamachenko, F. Kaap, M. Khabipov, R. Dolata, A. B. Zorin, and L. Grünhaupt, IEEE Trans. Appl. Supercond. 33, 1 (2023).
- ²²S. O. Peatáin, T. Dixon, P. J. Meeson, J. M. Williams, S. Kafanov, and Y. A. Pashkin, Supercond. Sci. Technol. 36, 045017 (2023).

- 23S.-H. Shin, M. Stanley, J. Skinner, S. E. de Graaf, and N. M. Ridler, IEEE Trans. Microwave Theory Techn. 72, 2193 (2024).
- ²⁴J. Skinner, M. Stanley, J. Urbonas, S. E. de Graaf, T. Lindström, and N. Ridler, in *IEEE MTT-S International Microwave Symposium* (IEEE, 2023), p. 561.
- ²⁵M. Stanley, M. Salter, J. Urbonas, J. Skinner, S.-H. Shin, S. E. de Graaf, and N. M. Ridler, IEEE Trans. Instrum. Meas. 73, 1500906 (2024).
- ²⁶G. Engen and C. Hoer, IEEE Trans. Microwave Theory Tech. **27**, 987 (1979).
- ²⁷M. Stanley, S. H. Shin, J. Skinner, J. Urbonas, and N. Ridler, in 53rd European Microwave Conference (EuMC) (IEEE, 2023), p. 150.
- ²⁸T. Hönigl-Decrinis, R. Shaikhaidarov, S. E. de Graaf, V. N. Antonov, and O. V. Astafiev, Phys. Rev. Appl. 13, 024066 (2020).
- ²⁹A. Remm, S. Krinner, N. Lacroix, C. Hellings, F. Swiadek, G. J. Norris, C. Eichler, and A. Wallraff, Phys. Rev. Appl. 20, 034027 (2023).
- ³⁰P. Roblin, Nonlinear RF Circuits and Nonlinear Vector Network Analyzers (Cambridge University Press, 2011).
- ³¹A. Ranadive, B. Fazliji, G. L. Gal, G. Cappelli, G. Butseraen, E. Bonet, E. Eyraud, S. Böhling, L. Planat, A. Metelmann, and N. Roch, arXiv:2406.19752 (2024).
- ³²M. Malnou, B. T. Miller, J. A. Estrada, K. Genter, K. Cicak, J. D. Teufel, J. Aumentado, and F. Lecocq, arXiv:2406.19476 (2024).
- ³³S. E. de Graaf, M. Stanley, and S.-H. Shin (2024). "In-operando microwave scattering-parameter calibrated measurement of a Josephson travelling wave parametric amplifier," Zenodo. https://doi.org/10.5281/zenodo.13268665